research papers

Measuring partial fluorescence yield using filtered detectors

T. D. Boyko,[a]* R. J. Green,[a] A. Moewes[a] and T. Z. Regier[b]

[a]Department of Physics and Engineering Physics, University of Saskatchewan, Saskatoon, Saskatchewan, Canada, and [b]Canadian Light Source Inc., University of Saskatchewan, Saskatoon, Saskatchewan, Canada. *E-mail: teak.boyko@usask.ca

Typically, X-ray absorption near-edge structure measurements aim to probe the linear attenuation coefficient. These measurements are often carried out using partial fluorescence yield techniques that rely on detectors having photon energy discrimination improving the sensitivity and the signal-to-background ratio of the measured spectra. However, measuring the partial fluorescence yield in the soft X-ray regime with reasonable efficiency requires solid-state detectors, which have limitations due to the inherent dead-time while measuring. Alternatively, many of the available detectors that are not energy dispersive do not suffer from photon count rate limitations. A filter placed in front of one of these detectors will make the energy-dependent efficiency non-linear, thereby changing the responsivity of the detector. It is shown that using an array of filtered X-ray detectors is a viable method for measuring soft X-ray partial fluorescence yield spectra without dead-time. The feasibility of this technique is further demonstrated using α-Fe$_2$O$_3$ as an example and it is shown that this detector technology could vastly improve the photon collection efficiency at synchrotrons and that these detectors will allow experiments to be completed with a much lower photon flux reducing X-ray-induced damage.

Keywords: XANES; partial fluorescence yield; photodiode.

1. Introduction

X-ray absorption spectroscopy (XAS), including the X-ray absorption near-edge structure (XANES) and extended X-ray absorption fine structure (EXAFS), is the most widely used X-ray spectroscopy technique. XAS has the capability of probing the electronic and crystal structure as well as the chemical specification of materials (Stöhr, 1992). During a XANES measurement, incident X-rays (in this case from a synchrotron source) excite core electrons into unoccupied states, at which point the system relaxes from these excited states emitting either fluorescence or scattered photons as well as Auger and photoelectrons. The intensity of the emitted photons or electrons is then recorded as a function of the incident X-ray energy and the resulting plot or spectrum is a measure of the linear attenuation coefficient. The linear attenuation coefficient, from the Beer–Lambert Law, is used to study several characteristics including the oxidation state (Pattanasiriwisawa et al., 2008) and the local bonding coordination (Perez-Huerta et al., 2008; Orton & Bilsborrow, 2008).

The most common techniques used to measure XANES spectra include the total electron yield (TEY) (Gudat & Kunz, 1972) and total fluorescence yield (TFY) (Jaklevic et al., 1977). The intensity of the TEY detector current I_g^{TEY} for an absorption measurement of edge g follows from equation (1)

assuming the material is very thick, where I_0 is the incident photon flux with energy E_i, $\eta_h^{\mathrm{e}}(E_i)$ is the electron yield, $\mu_h(E_i)$ is the attenuation coefficient, L_h is the escape depth of the emitted electrons for an absorption edge h, and $\mu(E_i)$ is the total attenuation coefficient. The intensity of the emitted photons from the material, I_g^{TFY} in (2), is similar to (1), where $\eta_h^{\mathrm{e}}(E_i, E_f)$ is the fluorescence yield efficiency and D_h is the average escape depth of the photons for the edge h with emission energy E_f. At this point the main difference between TEY and TFY is the escape depth of the electrons and the photons, respectively. For TEY the escape depth is limited to less than 10 nm, as opposed to TFY measurements where the photon escape depth has a range of $\sim$10–1000 nm (De Groot & Kotani, 2008). TEY and TFY measurements are also summed over all absorption edges with binding energy less than or equal to the incident photon energy, i.e. $g \geq h$. However, it is usually assumed that all emitted photons and electrons resulting from lower energy absorption are approximately constant and the sums in (1) and (2) collapse to a single term with a constant offset.

$$I_{g \geq h}^{\mathrm{TEY}}(E_i) \; \propto \; \sum_h I_0 \frac{\eta_h^{\mathrm{e}}(E_i)\mu_h(E_i)}{\mu(E_i) + (1/L_h)}, \qquad (1)$$

$$I_{g\geq h}^{\mathrm{TFY}}(E_i) \propto \sum_h I_0 \frac{\eta_h^{\mathrm{p}}(E_i, E_f)\mu_h(E_i)}{\mu(E_i) + (1/D_h)}. \tag{2}$$

The assumption that the non-resonant terms (the absorption edges with a binding energy lower than the absorption edge of interest) are constant is not always entirely valid. The TEY and TFY probe the linear attenuation coefficient only if these terms are approximately constant or very small compared with the resonant term (the absorption edge of interest). Obviously, the alternative to circumventing the possible issue is to measure the partial electron yield (PEY) or partial fluorescence yield (PFY). Then, it does not matter whether the non-resonant emission lines are constant, where PEY and PFY are described in equations (4) and (3), respectively. Even with restricting the XANES measurements to both PEY or PFY, there is still a significant shortcoming in that the intensity I_g^{PEY} and I_g^{PFY} may not be proportional to the attenuation coefficient $\mu_g(E_i)$ unless the concentration of the element of interest is very small (Tröger *et al.*, 1992; Bradley *et al.*, 2010). This non-linearity arises from the fact that the total attenuation coefficient can be approximated by a sum of attenuation coefficients of the individual absorption edges, $\mu(E_i) \simeq \sum_g \mu_g(E_i)$, implying that if the attenuation coefficient due to the element of interest is much smaller than the total attenuation coefficient then the denominator in equations (1) and (2) will be approximately constant. The measured intensity will then be proportional to the linear attenuation coefficient of the edge of interest since the attenuation coefficients of non-resonant absorption edges are approximately constant.

Measuring the emission from the non-resonant decay, which was previously assumed to be small and constant in the case of TFY, can circumvent this non-linear response or saturation. The measurement of the XANES using the non-resonant emission lines has been dubbed inverse PFY (IPFY) and is discussed in detail by Achkar *et al.* (2011). The IPFY follows from equation (5) for a non-resonant emission line $h \neq g$ and includes a constant offset C. It should be noted that IPFY probes the total attenuation coefficient, but for the edge of interest the total attenuation is effectively $\mu(E_i) \simeq \mu_g(E_i) + Q$, where Q is a constant,

$$I_g^{\mathrm{PEY}}(E_i) \propto I_0 \frac{\eta_g^{\mathrm{e}}(E_i)\mu_g(E_i)}{\mu(E_i) + (1/L_g)}, \tag{3}$$

$$I_g^{\mathrm{PFY}}(E_i) \propto I_0 \frac{\eta_g^{\mathrm{p}}(E_i, E_f)\mu_g(E_i)}{\mu(E_i) + (1/D_g)}, \tag{4}$$

$$I_{h\neq g}^{\mathrm{IPFY}}(E_i) = \frac{1}{I_{h\neq g}^{\mathrm{PFY}}(E_i)} \propto \mu(E_i) + C \simeq \mu_g(E_i) + Q. \tag{5}$$

The shortcomings of TFY and even PFY dictate that state-of-the-art XANES measurements require an energy-dispersive detector to separate the resonant and non-resonant emission. However, these detectors have a large cost per active area and are often plagued with long data acquisition times as well as small dynamic ranges introducing further non-linearity into the measured spectrum. Dead-time corrections can allow these detectors to operate at a much higher count rate, but in

the case of silicon drift detectors (SDDs) the input count rate needs to be well known, which can be difficult for soft X-rays. These corrections allow the count rate to be increased from a very restrictive range of ~ 20000 counts s^{-1} to upwards of ~ 100000 counts s^{-1}. These large count rates pale in comparison with the total number of fluorescence photons available, which are usually $> 10^{10}$ counts s^{-1} (total solid angle) making the efficiency of SDDs as small as 0.001% if a linear response is maintained. As better technology is continually developed for synchrotron facilities increasing the overall brightness of the X-ray beam, the current detector technology will be unable to take full advantage of the large photon flux.

Silicon photodiodes (PDs) are commonly employed as total fluorescence yield detectors on high-flux synchrotron beamlines (Dalba *et al.*, 1996; Goulon *et al.*, 2005; Baron *et al.*, 2006). These detectors are contrary to energy-dispersive detectors in that they have very large dynamic ranges and collect a very large solid angle acquiring TFY data quickly and efficiently, but provide no energy discrimination. However, if the specific fluorescence line structure is known, then there is a method to take full advantage of the extremely large efficiency of TFY detectors and still obtain the PFY spectrum. We develop and test a working PFY detector using filtered PDs and show that with two filtered TFY detectors it is possible to measure the PFY spectra of hemitite (α-Fe$_2$O$_3$) with a much larger collection efficiency and a significant reduction in the noise compared with an SDD detector.

2. Experimental set-up

There are many choices available for soft X-ray TFY detectors, but the photodiode is inexpensive, efficient and easy to implement when prototyping new detectors. PDs have almost 100% quantum efficiency for measuring soft X-rays due to the small penetration depth of low-energy X-rays (Gullikson *et al.*, 1996). Implementing PDs in a vacuum only requires that they be attached to an amplifier if the PDs are operated in photovoltaic mode. Fig. 1 shows the packaging for the PDs
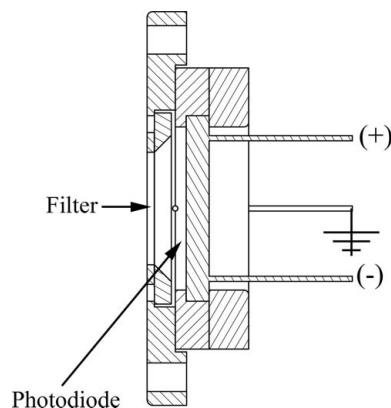

Figure 1
The PD detector design incorporating a metal filter that was used throughout the study. The metal foil, filter in this case, is placed in front of the silicon photodiode and provides both the PFY capability as well as shielding from electrons. The filter is also grounded.

used throughout this experiment. There is one key feature of the PD package design that is imperative for using PDs to measure XANES spectra. As mentioned, XANES measurements result in the emission of both photons and electrons. In order to avoid measuring the electrons being emitted during the XANES measurement, the PDs are encased in a non-conducting material with a grounded metal filter placed in front. In this arrangement the filter and casing prevent any influence from the photoelectrons and any electrons that are deposited in the metal filter are quickly sent to ground. The filters for the two PDs used here were free-standing aluminium and titanium, both 200 nm thick.

The Fe $2p$ XANES were measured on the Spherical Grating Monochromator (SGM) beamline located at the Canadian Light Source (Regier *et al.*, 2007). The material measured is a powder form of α-Fe$_2$O$_3$ that has been affixed to carbon tape and attached to the sample holder. None of the spectra have been calibrated on an absolute energy scale, although they were measured during the same experimental run and were normalized with respect to the incoming X-ray beam flux. The spectra, both from the SDD and PD detectors, were measured concurrently with 1.0 s integration times. The PFY and TFY spectra were measured using the PD array described above and an SDD detector for comparison. The specific arrangements of the detectors are important when it comes to comparing XANES spectra measured from different detectors. The SDD detector is at an angle of 25° and 48° for polar and azimuth directions, respectively. The two filtered PD detectors placed symmetrically with respect to the incoming X-ray beam are at 25° and 45° for the polar and azimuth directions with respect to the incident X-ray beam, respectively. The similar geometries of the SDD and PD detectors allow for the direct comparison of the measured spectra.

3. Results and discussion

In order to obtain PFY spectra from a TFY detector, a filter is placed in front of the TFY detector introducing non-linear energy dependence to the detector efficiency. Assuming the response of the bare TFY detector is constant or slowly changing with energy, the intensity read from the TFY detector when there are n emission lines present is described by equation (6), where $\mathbf{I}_n$ is the total spectrum from the TFY detector, and r_n is the efficiency at which the PFY spectrum $\mathbf{f}_n$ is measured. The deployment of these filters on an array of TFY detectors to measure PFY spectra is achieved as follows. If we first consider a single TFY detector, the measured TFY spectrum is modulated by the linear attenuation coefficient of the filter with respect to the emission line energy as expressed in equation (8). The response of s filtered TFY detectors, equation (7), would result in a system of s equations for the XANES of a material with n emission lines. Compacting equations (7) to (8) is achieved by substituting with matrices, $\underline{\mathbf{I}}$ for the set of measured intensities $\mathbf{I}_{g \geq n}^s(E_i)$, $\underline{R}$ for the responsivities r_n^s and $\underline{\mathbf{f}}$ for the set of PFY spectra $\mathbf{f}_n(E_i)$,

$$\mathbf{I}_n(E_i) = \begin{bmatrix} r_1, & r_2, & \ldots, & r_n \end{bmatrix} \begin{bmatrix} \mathbf{f}_1(E_i) \\ \mathbf{f}_2(E_i) \\ \ldots \\ \mathbf{f}_n(E_i) \end{bmatrix}, \quad (6)$$

$$\begin{bmatrix} \mathbf{I}_n^1(E_i) \\ \mathbf{I}_n^2(E_i) \\ \ldots \\ \mathbf{I}_n^s(E_i) \end{bmatrix} = \begin{bmatrix} r_1^1 & r_2^1 & \ldots & r_n^1 \\ r_1^2 & r_2^2 & \ldots & r_n^2 \\ \ldots & \ldots & \ldots & \ldots \\ r_1^s & r_2^s & \ldots & r_n^s \end{bmatrix} \begin{bmatrix} \mathbf{f}_1(E_i) \\ \mathbf{f}_2(E_i) \\ \ldots \\ \mathbf{f}_n(E_i) \end{bmatrix}, \quad (7)$$

$$\underline{\mathbf{f}} = \underline{R}^{-1} \underline{\mathbf{I}}. \quad (8)$$

Examining equation (8), the one basic requirement of the TFY detector array is that $\underline{R}$ must be invertible, which means that the responsivities of the filters must be linearly independent and there must be at least n filtered TFY detectors. Provided these criteria are met, it is in principle possible to measure the PFY spectra of any material. Additionally, there is a pronounced polarization dependence for the XANES spectra of a single crystal or if the electron transition does not involve spherical electron orbitals. As a result, the measured spectra will depend on the orientation of the detectors to a small extent. Scattering is another factor that can make the measured spectra appear different with respect to detector position. The result is that for linearly polarized X-rays a filtered TFY detector array is limited to evenly spaced detectors on an orthogonal concentric circle with respect to the incoming X-ray beam polarization.

While equation (8) shows that an array of filtered TFY detectors is theoretically capable of measuring PFY spectra, it is not clear whether different materials are capable of providing enough contrast between the measured XANES spectra to assemble a linearly independent responsivity matrix. Our test example here is hematite, α-Fe$_2$O$_3$, which has effectively three main emission lines when exciting the Fe $2p$ core electrons: oxygen $K\alpha$ and iron $L_{\alpha,\beta}$. The iron emission lines are so close in energy that they can be considered to have the same emission energy. Similarly, the third discounted emission line $M\zeta$ ($3s \rightarrow 2p$) is in between the O $K\alpha$ and Fe $L_{\alpha,\beta}$, and is grouped with both emission lines. The result is that there are only two emission lines in the energy range of interest when measuring the Fe $2p$ XANES spectrum, O and Fe for oxygen and iron, respectively. The total system of PDs is reduced from equation (8) to equation (9), where $\mathbf{I}_{\text{Fe}}^s$ is the measured spectrum, r_n^s is the responsivity and $\mathbf{f}_n$ is the PFY spectrum of emission n and PD s,

$$\begin{bmatrix} \mathbf{I}_{\text{Fe}}^1(E_i) \\ \mathbf{I}_{\text{Fe}}^2(E_i) \end{bmatrix} = \begin{bmatrix} r_{\text{O}}^1 & r_{\text{Fe}}^1 \\ r_{\text{O}}^2 & r_{\text{Fe}}^2 \end{bmatrix} \begin{bmatrix} \mathbf{f}_{\text{O}}(E_i) \\ \mathbf{f}_{\text{Fe}}(E_i) \end{bmatrix}. \quad (9)$$

The two filter materials arbitrarily chosen are aluminium (Al) and titanium (Ti) only because they were easily obtained; any filter material would suffice provided there is not a significant linear dependence between the linear attenuation coefficient. In fact, filters of the same material with different thickness would also have a non-linear dependence on the transmission.

Table 1
Final fit values $\tilde{r}_O$ and $\tilde{r}_{Fe}$ were obtained from the analysis presented below. The values r_O and r_{Fe} are from the CXRO database.

Photodiode filter	Fit gain response		Calculated atomic response	
	$\tilde{r}_O$	$\tilde{r}_{Fe}$	r_O	r_{Fe}
#1: aluminium foil	0.76	1.00	0.76	0.88
#2: titanium foil	0.22	0.40	0.22	0.41

Ideally, we would measure the responsivities of the Al and Ti filtered PDs and use the result to directly extract the PFY spectra from the Fe $2p$ XANES measurement. However, placing the filtered PDs in the direct path of the X-ray beam to measure the responsivities is not feasible at this time and therefore we employ an SDD detector at approximately the same geometry and use its measured PFY spectra to determine the response functions of the filtered PDs. This is achieved by creating a separate system of equations, this time by integrating the signal from the pre-edge and post-edge of the Fe and O PFY spectra. Equation (10) is then used to determine the response functions. Here, we use the pre- (695–700 eV) and post-edge (740–745 eV) regions, integrated over the flat region in order to mitigate the effect of noise, to determine the appropriate response functions that will generate the correct edge jump. This provides us now with an integrated value I^{pre} and I^{post} for the pre- and post-edge regions, respectively. The integrated PFY signals are labelled as G^{pre} and G^{post}. This approach can be applied to both XANES spectra from the Al and Ti filtered PDs to obtain the respective responsivity for these emission lines.

$$\begin{bmatrix} I_{Fe}^{pre} \\ I_{Fe}^{post} \end{bmatrix} = \begin{bmatrix} G_O^{pre} & G_{Fe}^{pre} \\ G_O^{post} & G_{Fe}^{post} \end{bmatrix} \begin{bmatrix} r_O \\ r_{Fe} \end{bmatrix}. \quad (10)$$

Table 1 shows the results of solving this system of equations. Comparing our results with the tabulated semi-empirical Henke data (Henke *et al.*, 1993) shows that they are very close to the atomic absorption data. This suggests that filtered PDs are capable of providing the necessary contrast to separate the PFY spectra from the TFY spectrum. The values of Table 1 have been normalized to the responsivity of the Fe emission line, the non-normalized values are then inserted into (9) giving us the final form, equation (11), which is used to extract the Fe and O PFY spectra from the raw PD spectra displayed in Fig. 2,

$$\begin{bmatrix} \mathbf{f}_O(E_i) \\ \mathbf{f}_{Fe}(E_i) \end{bmatrix} = \begin{bmatrix} 1.94 & 2.55 \\ 1.31 & 2.35 \end{bmatrix}^{-1} \begin{bmatrix} \mathbf{I}_{Fe}^1(E_i) \\ \mathbf{I}_{Fe}^2(E_i) \end{bmatrix}. \quad (11)$$

Having fit response functions for the two PDs, the PFY spectra of α-Fe$_2$O$_3$ are extracted from the two spectra measured with the filtered PDs. It should be noted that dark counts were subtracted from the PD spectra since the normalization of the spectra determined with the IPFY equation is only valid provided there is no offset in the spectra. Applying the responsivities of the Al and Ti filtered PDs using equations (8) and (9), Fig. 2 shows the PFY and IPFY spectra of α-Fe$_2$O$_3$. As

expected, all of the spectra, both PFY, IPFY and TFY, agree with the spectra measured using the SDD detector, but there are some differences in the ratios of the features. These differences are attributed to the saturation in the spectra measured with SDD and mixing of the discounted Fe $M\zeta$ emission line. The former demonstrates that PDs have the capability to remove all detector saturation from measured PFY spectra, but the latter is a problem that persists with finite-resolution PFY detectors. Interestingly, increasing the PD array size to three would provide the capability to measure this emission line and remove its contribution from the O and Fe PFY spectra. Moreover, the spectra are as good as or better with regard to the overall noise in the measurement owing to the significantly increased collection efficiency capability of the PD detectors since they can be placed arbitrarily closer to the sample. In this study we did not optimize the distance of the PDs with respect to the sample position, but better statistics are possible if the PDs are placed close to the sample. This cannot be said for the SDD detector, which was placed at the optimal position to avoid unacceptable saturation of the measured spectra.
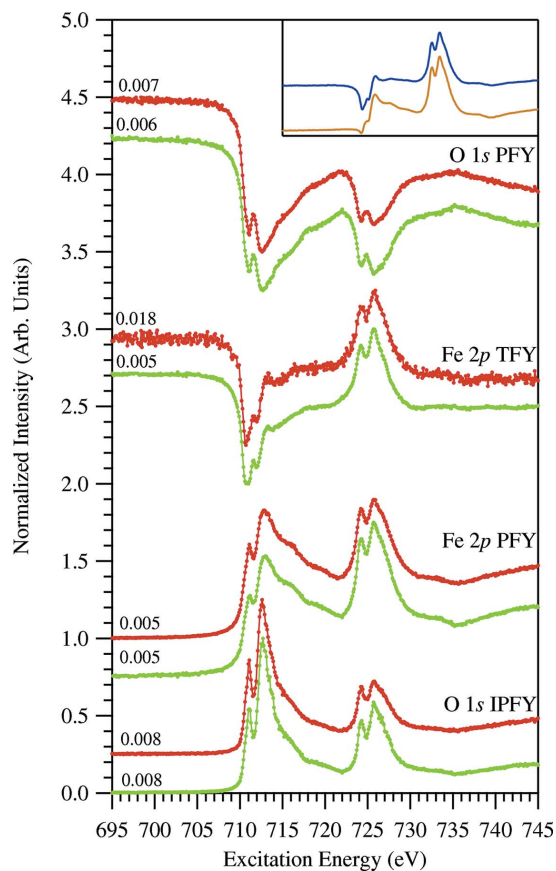
Figure 2
PFY spectra from the measured Fe $2p$ XANES of α-Fe$_2$O$_3$ using a SDD (red) detector and those extracted from the PDs (green) using equation (11) are displayed. The spectrum type is displayed above the spectra to the right, with the RMS noise value displayed to the left above their respective spectra. The inset panel in the upper right displays the raw spectra recorded from the PDs with an Al filter (blue) and the Ti filter (orange).

research papers

We have shown that two filtered PDs can be used to measure PFY spectra provided the response functions are known. In order to determine the response functions and be able to apply them for a filtered PD array in general with an arbitrary gain, one needs to realise the precise form of the PD response functions and devise a method to remove the specific gain of each individual detector. The gain convoluted response functions can be measured directly by placing the detector in the X-ray beam, assuming that the X-ray beam contains no higher-order light. This produces the response function matrix $\tilde{R}$ in equation (12), which can be easily decomposed to produce the gain matrix $\underline{C}$ and the pure response function matrix $\underline{R}$ in that $\tilde{\underline{R}} = \underline{C}\underline{R}$ with n emission lines and s PDs. Although the response functions can be measured directly for a particular detector set-up using a tunable X-ray source such as a synchrotron, one would like to arbitrarily change the gain of each detector since each filtered PD will have a different efficiency dependent on the emission line energy and intensity.

Normalizing the measured response functions for the filtered PD detectors is achieved by using a reference fluorescence line. Ideally, one would use a reference emission line that is appropriate for the energy range of the beamline being used; for our case we will choose graphite and use the C $K\alpha$ emission line at 277 eV labelled with subscript C. This same emission line must be used for normalization throughout the measurements; however, it is not required to choose the emission line ahead of time and any emission line can be used provided it has a single emission energy value. Equation (13) follows from this, where $\bar{R}$ is the array of normalized response functions. The normalized response functions are then applied by simply measuring the intensity of the fluorescence signal of the reference emission line, without changing the gain of the detector, and using the intensity to normalize the XANES spectra of interest as in equation (14). The normalized response functions in (13) are then applied to the XANES spectra that have been normalized to the reference emission line as in equation (15). The result is that the true PFY spectra are extracted independent of the gain of the detector, but scaled by a constant related to the reference emission line as in equation (16). This will still provide invariance of the spectra regardless of PD degradation or amplifier settings.

$$\tilde{\underline{R}} = \begin{bmatrix} c^1 & 0 & \ldots & 0 \\ 0 & c^2 & \ldots & 0 \\ \ldots & \ldots & \ldots & \ldots \\ 0 & 0 & \ldots & c^n \end{bmatrix} \begin{bmatrix} r_1^1 & r_2^1 & \ldots & r_n^1 \\ r_1^2 & r_2^2 & \ldots & r_n^2 \\ \ldots & \ldots & \ldots & \ldots \\ r_1^s & r_2^s & \ldots & r_n^s \end{bmatrix}, \quad (12)$$

$$\bar{R} = \begin{bmatrix} r_1^1/r_C^1 & r_2^1/r_C^1 & \ldots & r_n^1/r_C^1 \\ r_1^2/r_C^2 & r_2^2/r_C^2 & \ldots & r_n^2/r_C^2 \\ \ldots & \ldots & \ldots & \ldots \\ r_1^s/r_C^s & r_2^s/r_C^s & \ldots & r_n^s/r_C^s \end{bmatrix}, \quad (13)$$

$$\begin{bmatrix} \mathbf{I}_{PD}^{1\prime} \\ \mathbf{I}_{PD}^{2\prime} \\ \ldots \\ \mathbf{I}_{PD}^{s\prime} \end{bmatrix} = \begin{bmatrix} I_C^1 & 0 & \ldots & 0 \\ 0 & I_C^2 & \ldots & 0 \\ \ldots & \ldots & \ldots & \ldots \\ 0 & 0 & \ldots & I_C^s \end{bmatrix}^{-1} \begin{bmatrix} \mathbf{I}_{PD}^1 \\ \mathbf{I}_{PD}^2 \\ \ldots \\ \mathbf{I}_{PD}^s \end{bmatrix}, \quad (14)$$

$$\begin{bmatrix} \mathbf{I}_{PD}^{1\prime} \\ \mathbf{I}_{PD}^{2\prime} \\ \ldots \\ \mathbf{I}_{PD}^{s\prime} \end{bmatrix} = \frac{1}{f_C} \begin{bmatrix} r_1^1/r_C^1 & r_2^1/r_C^1 & \ldots & r_n^1/r_C^1 \\ r_1^2/r_C^2 & r_2^2/r_C^2 & \ldots & r_n^2/r_C^2 \\ \ldots & \ldots & \ldots & \ldots \\ r_1^s/r_C^s & r_2^s/r_C^s & \ldots & r_n^s/r_C^s \end{bmatrix} \begin{bmatrix} \mathbf{f}_1 \\ \mathbf{f}_2 \\ \ldots \\ \mathbf{f}_n \end{bmatrix}, \quad (15)$$

$$\mathbf{I}_{PD}' = \frac{1}{f_C} \bar{\underline{R}} \mathbf{F} \Rightarrow \mathbf{F} \propto \bar{\underline{R}}^{-1} \mathbf{I}_{PD}'. \quad (16)$$

4. Conclusion

The progress in developing brighter X-ray sources motivates the need for more efficient detectors capable of handling a larger photon flux. We have developed and tested a method to measure PFY and IPFY spectra using filtered TFY detectors. The measurements of the Fe $2p$ XANES on α-Fe_2O_3 show that by using Ti and Al foil filters the PFY spectra can be extracted with comparable or improved statistical quality over conventional SDD detectors. This method can easily be applied to any TFY detector and be used in conjunction with energy-dispersive detectors to provide an alternative more efficient means of measuring the PFY and IPFY spectra at intense X-ray sources. Furthermore, a method has been put forth to extract the PFY spectra independent of the specific gain of the detector and we show that any array of filtered TFY detectors provides an inexpensive and efficient detector system capable of measuring soft X-ray PFY and IPFY spectra.

References

Achkar, A. J., Regier, T. Z., Wadati, H., Kim, Y. J., Zhang, H. & Hawthorn, D. G. (2011). *Phys. Rev. B*, **83**, 081106.

Baron, A. Q. R., Kishimoto, S., Morse, J. & Rigal, J.-M. (2006). *J. Synchrotron Rad.* **13**, 131–142.

Bradley, J. A., Yang, P., Batista, E. R., Boland, K. S., Burns, C. J., Clark, D. L., Conradson, S. D., Kozimor, S. A., Martin, R. L., Seidler, G. T., Scott, B. L., Shuh, D. K., Tyliszczak, T., Wilkerson, M. P. & Wolfsberg, L. E. (2010). *J. Am. Chem. Soc.* **132**, 13914–13921.

Dalba, G., Fornasini, P., Soldo, Y. & Rocca, F. (1996). *J. Synchrotron Rad.* **3**, 213–219.

De Groot, F. & Kotani, A. (2008). *Core Level Spectroscopy of Solids.* Boca Raton/London: Taylor and Francis/CRC Press.

Goulon, J., Rogalev, A., Goujon, G., Gauthier, C., Moguiline, E., Solé, A., Feite, S., Wilhelm, F., Jaouen, N., Goulon-Ginet, C., Dressler, P., Rohr, P., Lampert, M.-O. & Henck, R. (2005). *J. Synchrotron Rad.* **12**, 57–69.

Gudat, W. & Kunz, C. (1972). *Phys. Rev. Lett.* **29**, 169–172.

Gullikson, E. M., Korde, R., Canfield, L. R. & Vest, R. E. (1996). *J. Electron Spectrosc. Relat. Phenom.* **80**, 313–316.

Henke, B. L., Gullikson, E. M. & Davis, J. C. (1993). *At. Data Nucl. Data Tables*, **54**, 181–342.

Jaklevic, J., Kirby, J. A., Klein, M. P., Robertson, A. S., Brown, G. S. & Eisenberger, P. (1977). *Solid State Commun.* **23**, 679–682.

Orton, B. R. & Bilsborrow, R. (2008). *J. Synchrotron Rad.* **15**, 641–647.

Pattanasiriwisawa, W., Siritapetawee, J., Patarapaiboolchai, O. & Klysubun, W. (2008). *J. Synchrotron Rad.* **15**, 510–513.

Pérez-Huerta, A., Cusack, M., Janousch, M. & Finch, A. A. (2008). *J. Synchrotron Rad.* **15**, 572–575.

Regier, T., Krochak, J., Sham, T. K., Hu, Y. F., Thompson, J. & Blyth, R. I. R. (2007). *Nucl. Instrum. Methods Phys. Res. A*, **582**, 93–95.

Stöhr, J. (1992). *NEXAFS Spectroscopy.* Berlin: Springer.

Tröger, L., Arvanitis, D., Baberschke, K., Michaelis, H., Grimm, U. & Zschech, E. (1992). *Phys. Rev. B*, **46**, 3283–3289.